Volume 12 Number 2
Journal of Advances in Physics

Microstructural analysis for Sn-Bi-Sb-In alloy prepared by rapid solidification

S. Mosaad [(1,*)], A. R. Mohamed[2], Mustafa Kamal[3]
[(1,*)] Physics Department, Faculty of Science, Suez Canal University, Egypt
saramosaad@windowslive.com
[2] Physics Department, Faculty of Science, Port Said University, Egypt
raoufahmed@yahoo.com
[3] Metal Physics lab. Physics Department, Faculty of Science, Mansoura University, Egypt
kamal42200274@yahoo.com

Abstract

In the present study, Sn_{70-X} at.% -Bi_{15} at.% -Sb_{15} at.%- In_x at.% alloy (x= 0, 2, 4, 6), were prepared by melt spinning technique. Optical microscopy, scanning electron microscopy combined with energy dispersive X-ray analysis (SEM-EDX), X-ray diffraction analysis (XRD), and Vickers microhardness (Hv); were used to characterize the phase transformation and the microstructure evolution. The results contribute to the understanding of the microstructure evolution in alloys of the type prepared by melt spinning technique. This work reports on a comparative study of the rapidly solidified, in order to compare the microhardness and microstructural analysis.

Keywords

Rapid Solidification (RS); Lead Free Solder Alloys; Sn-Bi-Sb, X-Ray Diffraction Analysis (XRD), Scanning Electron Microscope; Energy Dispersive X-Ray, Vickers microhardness (Hv).

Academic Discipline and Sub-Disciplines

Physics; Solid State Physics

SUBJECT CLASSIFICATION

Solder alloy

TYPE (METHOD/APPROACH)

Experimental

Introduction

In the electronics industry lead-tin (Pb-Sn) solder is a very important material. Due to the harmful effects of Pb the use of the Pb-Sn solder alloys are being avoided and new Pb-free solder alloys are used for electronic applications. Several alternate solder alloys are investigated and their various properties are studied [1-3]. Rapid solidification of metallic alloys results in refined microstructures with reducing microsegregation and improves mechanical properties of the final products as compared to normal castings. The rapidly solidified Sn-based solders by melt spinning have proved to be suitable for soldering at low temperature and short soldering duration [4-6].

The properties and performance of lead-free solder alloys such as fluidity and wettability may be controlled by alloy composition and solidification microstructure. The hardness of the bearing and the inter-relation between resistance to deformation and conformability is the main consideration. High-tin lead free alloys are used in applications where high unit loads and high temperatures are encountered. With heavy fluctuating loads such as that encountered in internal combustion engines, however, experience has shown that the softer alloys are superior in spite of lower fatigue properties. The reason is that they bound up with greater ability to conform to shaft deflection.

This work aims to understand the different intermetallic alloys that are formed in Sn_{70-x}-Bi_{15}-Sb_{15}-In_x alloys (where x= 0 , 2, 4, and 6 in at. %) . Also, some light are exposed on the homogenous of elements which used in preparing alloys and the intermetallic compound that formed and it's mechanical properties.

Experimental procedures

The materials used in the present work are Sn, Sb, Bi, and In fragments, with purity better than 99.99% produced by a single copper roller (200 mm in diameter) melt-spinning technique which described previously in some details [7-10]. The process parameters such as the ejection temperature, and the linear speed of the wheel were fixed at 873 K and 30.4 ms^{-1} respectively. X-ray diffraction analysis (XRD) was carried out with a XPERT-PRO X-ray diffractometer, using Cu-Kα radiation (λ = 1.5406 Å). The polished and etched samples were observed using an optical microscope (Olympus Model: PMG 3) with the objective of determining the microstructural evolution. The microstructure analysis was carried out on a scanning electron microscope (SEM) of type (FEI Inspect-S50) operate at 30Kv with high resolution 3nm. Quantx Bruker EDS spectrometer System is a full-featured X-Ray Microanalysis System (EDX/EDS) for SEM result. The elastic moduli of melt-spun ribbons were examined in air atmosphere with a modified dynamic resonance method [11]. The hardness of the melt-spun ribbons was measured using a digital Vickers microhardness tester (model SHIMADZU HMV) [12]. The test carried out at load 98.07mN (10 gram force) with loading time 15 sec.

ISSN 2347-3487
Volume 12 Number 2
Journal of Advances in Physics

2- Results and Discussion

2.1 Structure

Figure (1) shows the X-ray diffraction pattern for as-quenched melt-spun of Sn_{70-x}-Bi_{15}-Sb_{15}-In_x alloys (where x= 0 , 2, 4, and 6 in at. %). The experimental observed interplanar spacing's of the first few strong reflections are tabulated in Table (1). The pattern can be indexed in terms of the co-existence of Tetragonal Sn, Rhombohedral Sb and Bi phases, Tetragonal In, and intermediate compounds such as Rhombohedral SnSb and Orthorhombic InSn, Tetragonal Bi_3In_5, Hexagonal $In_{0.2}Sn_{0.8}$. The XRD for Sn_{70}-Bi_{15}-Sb_{15} alloy is shown in Figure 1(a), Sn, Bi and Sb are precipitated as indicated and SnSb Intermetallic compound is appeared. The unit cell of β-Sn is body centered tetragonal (S.G.: I41/amd). The crystal structure of Bi is Rhombohedral-hexagonal (S.G.: R3m), the unit cell of Sb is Rhombohedral (S.G.: R-3m) and the unit cell of SbSn is Rhombohedral (S.G.: R-3m).

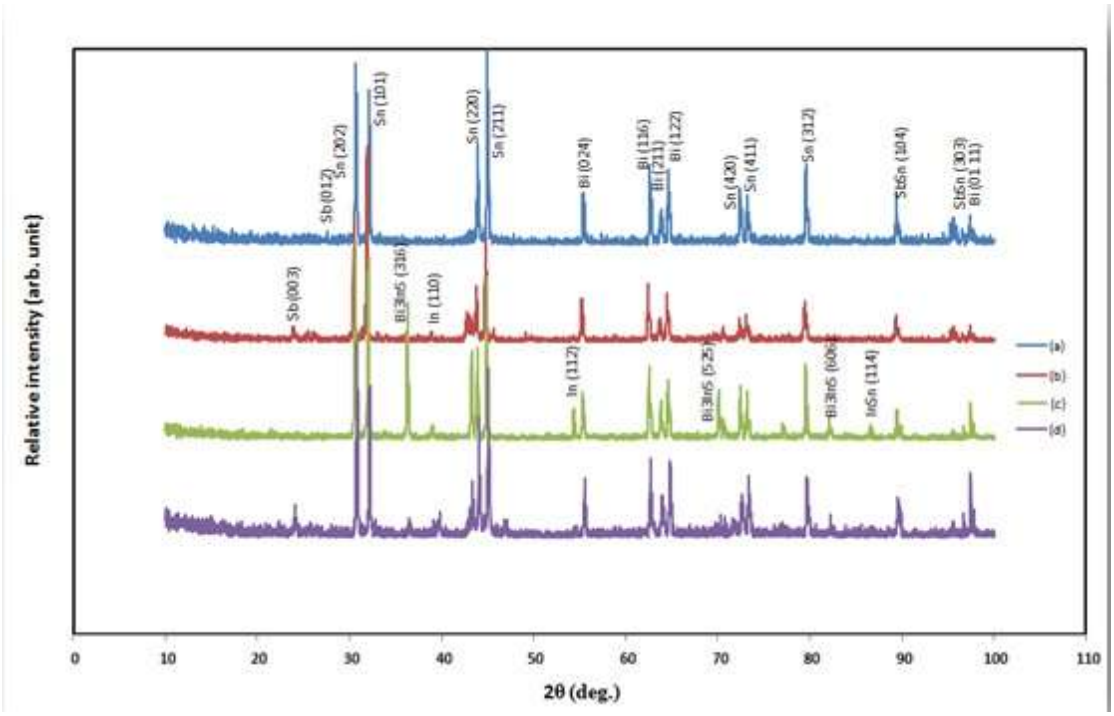

Fig.1. The XRD patterns for as-quenched melt-spun alloys. (a) Sn_{70}-Bi_{15}-Sb_{15}; (b) Sn_{68}-Bi_{15}-Sb_{15}-In_2; (c) Sn_{66}-Bi_{15}-Sb_{15}-In_4; and (d) Sn_{64}-Bi_{15}-Sb_{15}-In_6.

Figure 1(b) shows Sn_{68}-Bi_{15}-Sb_{15}-In_2 alloy, in which a formation of new Intermetallic compounds and these are, InSb with Orthorhombic crystal structure (S.G.: Pmmn), and Bi_3In_5 Intermetallic phase with Tetragonal unit cell (S.G.: 14/mcm). Also, the Sn, In, Bi, and Sb phases are exist in their positions.

By Increasing In at.% as in Sn_{66}-Bi_{15}-Sb_{15}-In_4 alloy (Figure 1(c)) It is quite obvious that, a new phase is formed, $In_{0.2}Sn_{0.8}$ with Hexagonal crystal structure (S.G.: P6/mmm). SnSb Intermetallic phase returns to appear again in the absence of Sb phase. (Figure 1(d)) is for Sn_{64}-Bi_{15}-Sb_{15}-In_6 alloy. In this alloy, all intermediate phases are formed except $In_{0.2}Sn_{0.8}$. Particle size can be calculated for each present phase using scherrer's equation [11]. The detail of XRD analysis is shown in Table 1.

Table 1. The XRD patterns details for as-quenched melt-spun alloys. Sn_{70}-Bi_{15}-Sb_{15}; Sn_{68}-Bi_{15}-Sb_{15}-In_2; Sn_{66}-Bi_{15}-Sb_{15}-In_4 and; Sn_{64}-Bi_{15}-Sb_{15}-In_6.

Alloy	Phase present	hkl	The lattice parameter for each phase				Particle size (μm)	Crystal structure
			a (Å)	c (Å)	v (Å^3)	c/a		
Sn_{70}-Bi_{15}-Sb_{15}	Sn	200	5.8177	3.1697	107.2854	0.5448	4.1914	Tetragonal (S.G.: I41/amd)
	Bi	012	4.6166	11.8450	218.6304	2.5657	6.5431	Rho.-hex. (S.G.: R3m)
	Sb	003	4.4346	11.2270	191.2017	2.5316	8.0810	Rho. (S.G.: R-3m)

	SbSn	021	4.2007	4.5947	70.2147	1.0937	6.8632	Rho. (S.G.: R-3m)
Sn_{68}-Bi_{15}-Sb_{15}-In_2	Sn	200	5.8489	3.1922	109.2093	0.5457	4.3061	Tetragonal (S.G.: I41/amd)
	Bi	012	4.5067	11.9018	209.3425	2.6409	14.9243	Rho.-hex. (S.G.: R3m)
	Sb	003	4.2530	11.1560	174.7518	2.6230	5.4713	Rho. (S.G.: R-3m)
	In	110	3.3035	4.9007	53.4827	1.4835	9.8187	Tetragonal (S.G.: 14/mmm)
	InSb	201	5.7656	5.4048	3.0487	95.0076	8.3070	Ortho. (S.G.: Pmmn)
	Bi_3In_5	312	8.4704	12.6834	910.0141	1.4973	5.8683	Tetragonal (S.G.: 14/mcm)
Sn_{66}-Bi_{15}-Sb_{15}-In_4	Sn	200	5.8272	3.1789	107.9488	0.5455	4.227	Tetragonal (S.G.: I41/amd)
	Bi	012	4.5544	11.7411	210.9147	2.5779	1.0841	Rho.-hex. (S.G.: R3m)
	In	110	3.2522	4.9437	52.2916	1.5200	5.1361	Tetragonal (S.G.: 14/mmm)
	InSb	201	5.8034	5.5428	3.0134	96.9348	5.8903	Ortho. (S.G.: Pmmn)
	Bi_3In_5	312	8.5575	12.6935	929.5698	1.4833	6.0705	Tetragonal (S.G.: 14/mcm)
	$In_{0.2}Sn_{0.8}$	001	3.1490	3.1067	26.6803	0.9865	0.6296	Hexagonal (S.G.: P6/mmm)
Sn_{64}-Bi_{15}-Sb_{15}-In_6	Sn	200	5.7836	3.1662	105.9116	0.5474	4.229	Tetragonal (S.G.: I41/amd)
	Bi	012	4.5329	11.8756	211.3194	2.6198	5.5759	Rho.-hex. (S.G.: R3m)
	Sb	003	4.2222	11.0679	170.8711	2.6213	5.4713	Rho. (S.G.: R-3m)
	In	110	3.2493	4.9372	52.1283	1.51947	7.3256	Tetragonal (S.G.: 14/mmm)
	SbSn	021	4.2349	5.4370	84.4468	1.2838	5.6397	Rho. (S.G.: R-3m)
	InSb	201	5.8907	5.2412	2.9453	90.9381	4.2865	Ortho. (S.G.: Pmmn)
	Bi_3In_5	312	8.4001	12.8437	906.2875	1.5289	6.2893	Tetragonal (S.G.: 14/mcm)

2.2 Sample preparation

Specimens were mounted at room temperature using acrylics castable mounting materials (cold resin). Then, the specimens were mechanically ground using emery papers up to 1200 grade. Scratches from the abrasive papers are removed by polishing specimens for several minutes on a wheel covered with a short-nap cloth impregnated with 0.25 µm diamond paste. The samples rinsed and degreased with acetone, and then etched using 5 ml nitric acid + 2ml HCL in 100 ml methanol for 45s.

2.3 Microstructural characteristics

In the present investigation, rapidly quenched alloys Sn_{70-x}-Bi_{15}-Sb_{15}-In_x (x= 0 , 2, 4, and 6 in at. %) were examined by optical microscope, scanning electron microscope and energy dispersive spectroscopy x-ray. Knowledge of the microstructure of a material, which is the number of phases present, their distribution, volume fraction, shape, and size, are essential since many properties are structure sensitive, e.g. mechanical and electrical properties. Thus this section is concerned with the study of the microstructure of the alloys which have been prepared to explain their properties.

2.3.1 Optical microscopy

A more detailed view of the alloys surfaces is shown in figure (2) where optical microscopy images show that the surfaces have different structures for each prepared alloy.

2.3.2 SEM and EDS

Figure (3) shows the SEM image of alloy $Sn_{70}Bi_{15}Sb_{15}$, EDS Spectra of the points 1 and 6 of EDS spot analysis and EDS map analysis of the alloying elements shows a homogenous distributions of the alloying elements in alloy $Sn_{70}Bi_{15}Sb_{15}$. Figures (3a1, 3a2) shows the formation of the soft phase (Sn) nearly continuous network in the $Sn_{70}Bi_{15}Sb_{15}$ alloy. The grains in the middle of ribbon, which looks like a rod in shape, are extended along the length direction (the direction of the linear momentum of the wheel). The number of grains per μm^2 was found to be 418, total projected area is 79 μm^2, mean grain area is $190*10^{-15}$ m^2, mean grain size is 0.42 µm, total grain volume is $42*10^{-21}$ m^3.

ISSN 2347-3487
Volume 12 Number 2
Journal of Advances in Physics

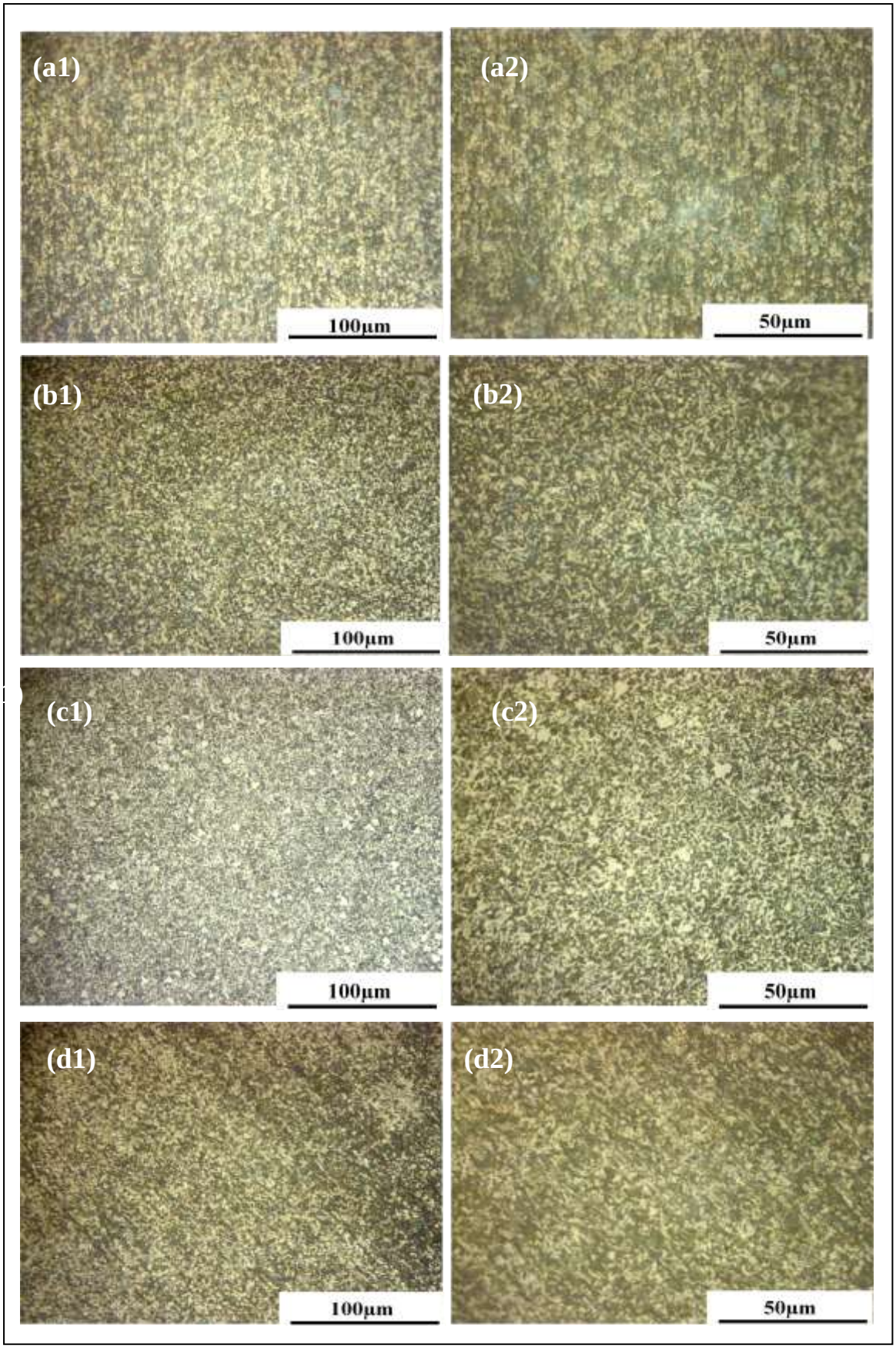

Fig. 2 Optical Microscopy images for (a) Sn_{70}-Bi_{15}-Sb_{15}; (b) Sn_{68}-Bi_{15}-Sb_{15}-In_2; (c) Sn_{66}-Bi_{15}-Sb_{15}-In_4; and (d) Sn_{64}-Bi_{15}-Sb_{15}-In_6.

Figures (4a1, 4a2) show the SEM image for alloy $Sn_{68}Bi_{15}Sb_{15}In_2$. Figures (4b1, 4b2) are shown EDS Spectra of the points 1 and 6 of EDS spot analysis and figure 4c is the EDS map analysis of the alloying elements.

Figures (5a1, 5a2) show the SEM image for alloy $Sn_{66}Bi_{15}Sb_{15}In_4$, EDS Spectra of the points 1 and 6 of EDS spot analysis shown in figures (5b1, 5b2) and EDS map analysis of the alloying elements showing the homogenous distributions of the alloying elements for alloy $Sn_{66}Bi_{15}Sb_{15}In_4$ shown in figure 5c.

Figures (6a1,6a2) show the SEM image for alloy $Sn_{66}Bi_{15}Sb_{15}In_4$, figures (6b1, 6b2) show EDS Spectra of the points 1 and 6 of EDS spot analysis. Figure 6c show EDS map analysis of the alloying elements showing the homogenous distributions of the alloying elements for alloy $Sn_{66}Bi_{15}Sb_{15}In_4$.

Table (2) EDS spot analysis of the points 1, 2, 3, 4, 5 and 6 in the SEM images for all alloys. Table (3) shows the variation of number of grains and the grain size for different alloys. Crystallite and grain are both single crystals; a crystallite is a single crystal in powder form but a grain is a single crystal within a bulk/thin film.

A particle is also thought of as an agglomerate, small enough in size to not consider it as a bulk or thin film, but composed of 2 or more individual crystallites. From the figures, it shows that the microstructures were composed of elongated grains, a few microns in width and several microns in length. Also evident in the micrographs was a highly density of extinction contours which indicated that considerable internal strain was introduced in the material as a result of melt spinning.

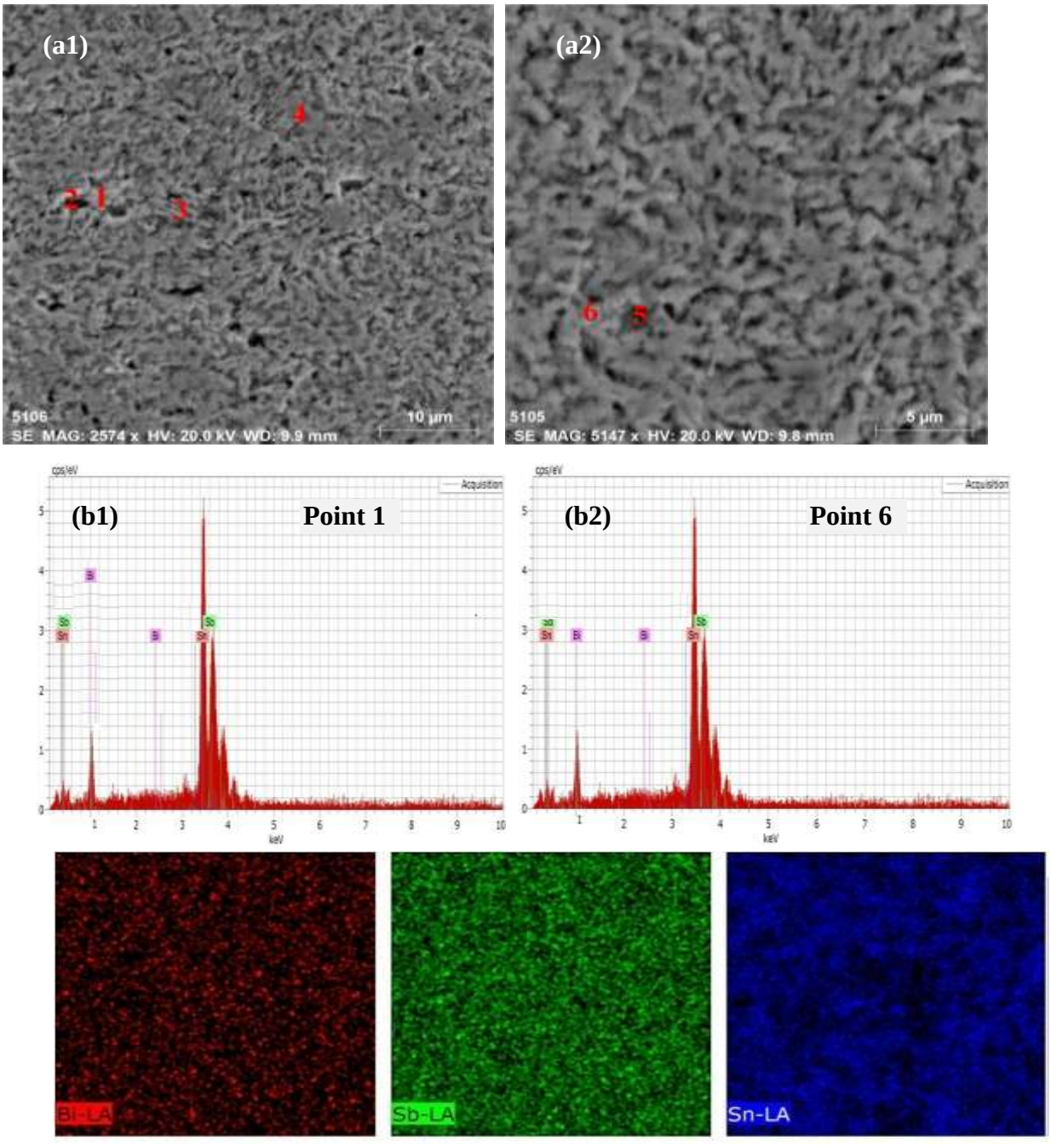

Fig. 3 (a) SEM images (b) EDS spectra of the points 1 and 6 and (c) EDS map analysis for $Sn_{70}Bi_{15}Sb_{15}$ alloy.

ISSN 2347-3487
Volume 12 Number 2
Journal of Advances in Physics

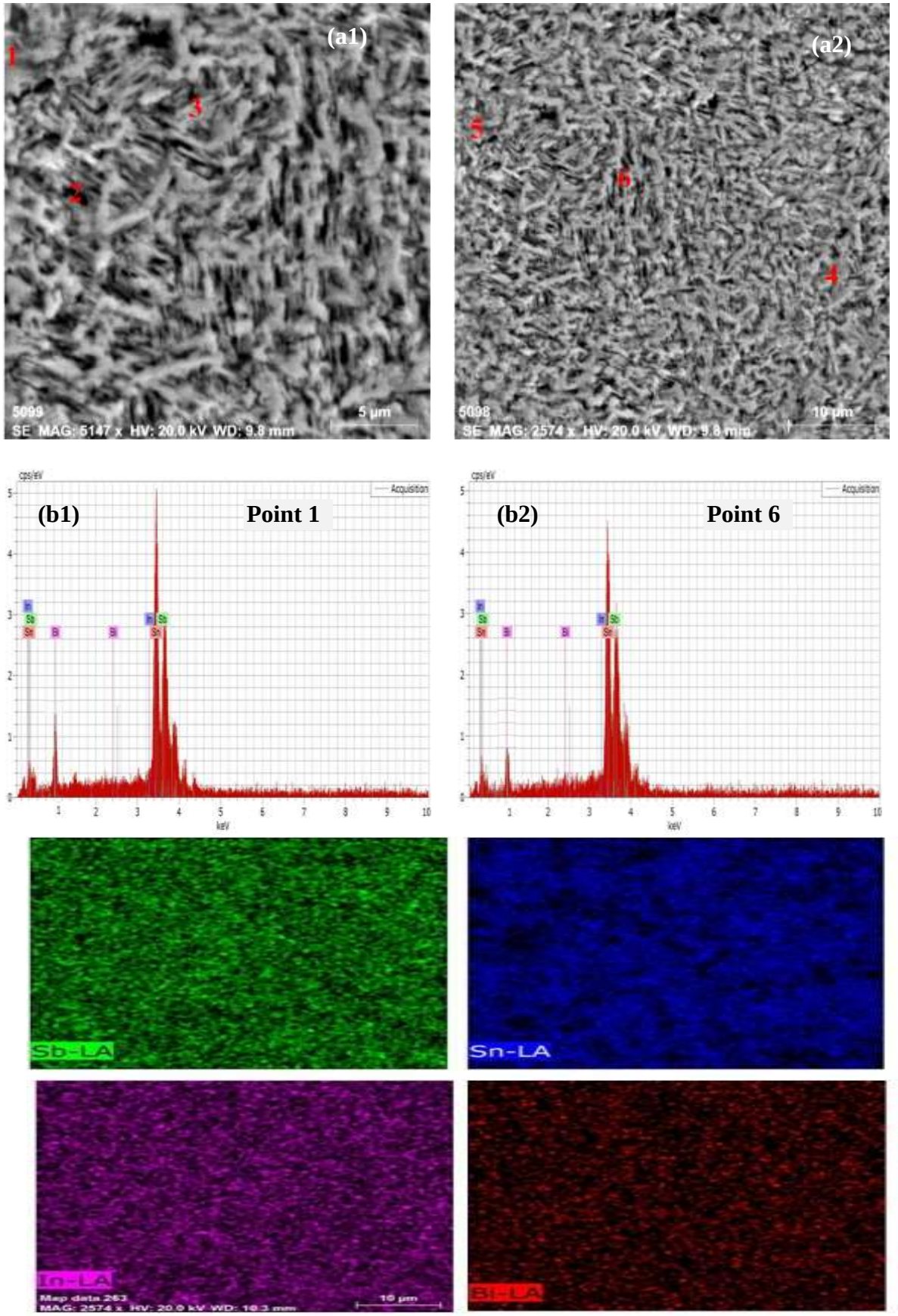

Fig. 4 (a) SEM images (b) EDS spectra of the points 1 and 6 and (c) EDS map analysis for $Sn_{68}Bi_{15}Sb_{15}In_2$ alloy.

ISSN 2347-3487
Volume 12 Number 2
Journal of Advances in Physics

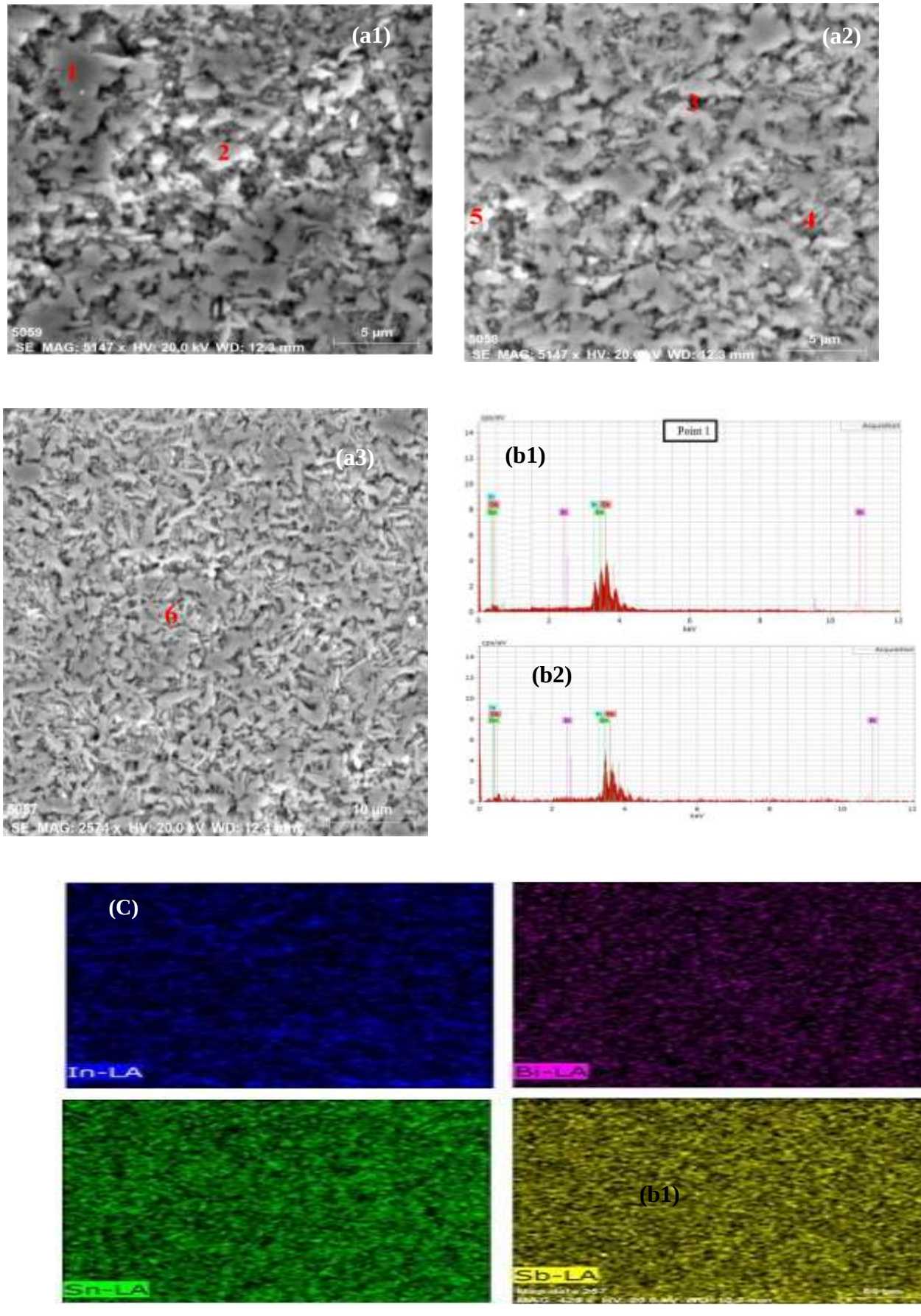

Fig. 5 (a) SEM images (b) EDS spectra of the points 1 and 6 and (c) EDS map analysis for $Sn_{66}Bi_{15}Sb_{15}In_4$ alloy.

ISSN 2347-3487
Volume 12 Number 2
Journal of Advances in Physics

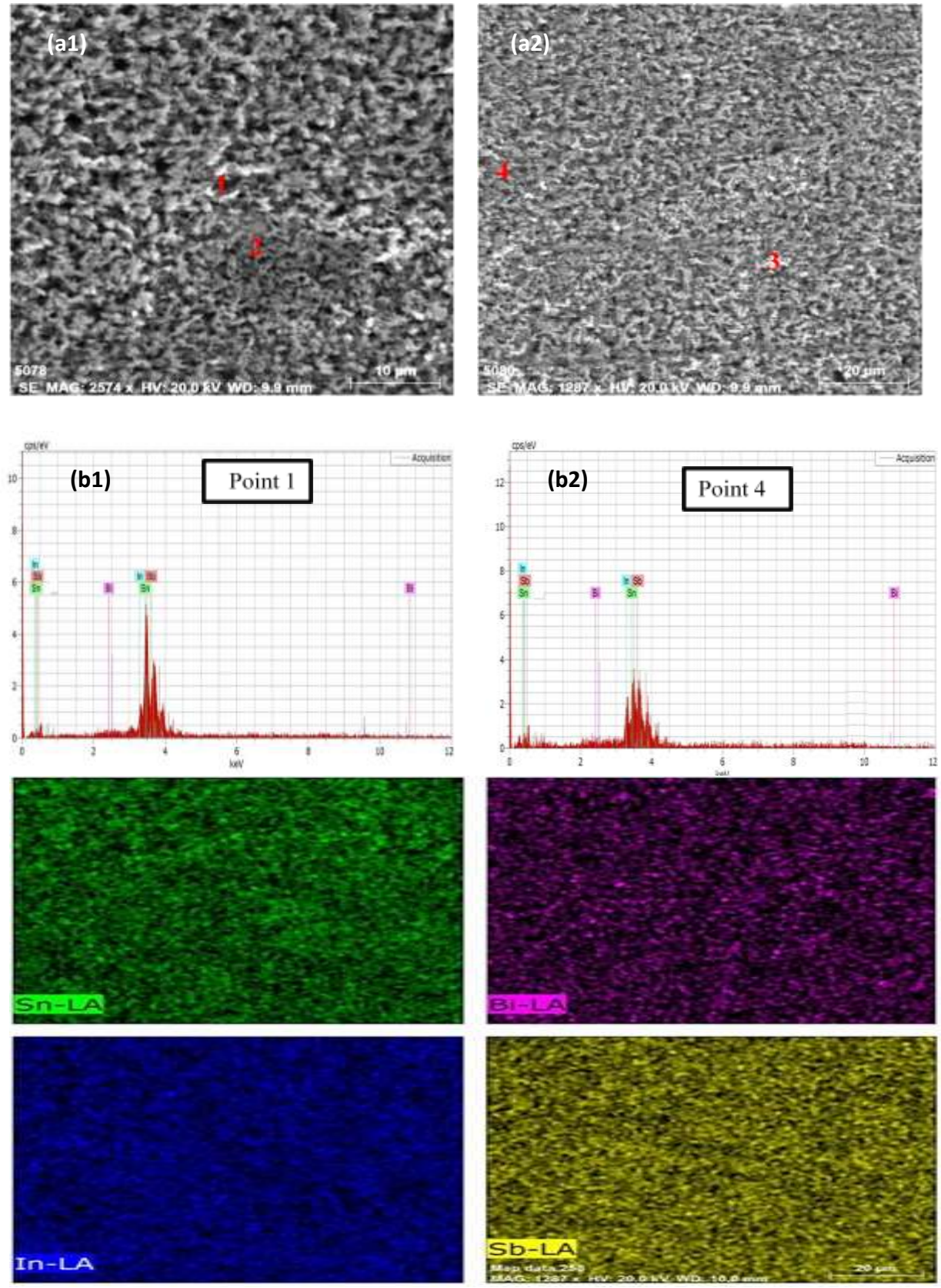

Fig. 6 (a) SEM images (b) EDS spectra of the points 1 and 6 and (c) EDS map analysis for $Sn_{64}Bi_{15}Sb_{15}In_6$ alloy.

Table 2. EDS spot analysis of the points 1, 2, 3, 4, 5 and 6 in the SEM images for all prepared alloys.

Alloy	Element	Wt.%					
		Point 1	Point 2	Point 3	Point 4	Point 5	Point 6
$Sn_{70}Bi_{15}Sb_{15}$	Sn	70.07	81.99	91.02	90.60	64.98	79.71
	Sb	14.42	5.57	0.0	0.0	16.10	6.84
	Bi	4.49	5.18	6.53	7.46	3.42	6.57
$Sn_{68}Bi_{15}Sb_{15}In_2$	Sn	59.85	65.17	36.55	86.51	75.64	65.95
	Sb	19.87	18.77	34.68	5.01	11.85	15.87
	In	1.46	3.20	1.28	3.54	4.52	2.23
	Bi	18.82	11.77	27.49	4.93	7.94	15.95
$Sn_{66}Bi_{15}Sb_{15}In_4$	Sn	40.53	43.29	43.81	34.33	45.46	43.83
	Sb	36.46	33.87	33.10	46.8	30.72	35.28
	In	2.87	11.13	4.13	7.34	13.95	10.34
	Bi	20.14	11.71	18.96	11.53	9.87	10.56
$Sn_{64}Bi_{15}Sb_{15}In_6$	Sn	38.37	50.59	46.93	63.65		
	Sb	32.06	22.03	27.51	14.27		
	In	24.49	14.99	22.85	17.34		
	Bi	5.08	11.05	2.71	3.51		

Table 3. Grain details for all prepared alloys.

Alloy	Number of grains	Total projected area (μm^2)	Mean grain area (10^{-15} m^2)	Mean grain size (μm)	Total grain volume (10^{-21} m^3)
Sn_{70}-Bi_{15}-Sb_{15}	418	79	190	0.42	42
Sn_{68}-Bi_{15}-Sb_{15}- In_2	958	78	81	0.27	57
Sn_{66}-Bi_{15}-Sb_{15}- In_4	878	223	254	0.42	167
Sn_{64}-Bi_{15}-Sb_{15}- In_6	1154	118	102	0.30	81

2.3.3 Mechanical Properties

Firstly, we study Vickers microhardness analysis. The indentations were made in two directions along the width of the ribbon (X-direction) and along the length of the ribbon (Y- direction which is the direction of the linear momentum of the wheel). The test carried out using SHIMADZU Model, at load 98.07mN (10 gram force) and loading time is 15 sec. The hardness test involves indenting a material by a process of plastic deformation which approximately 8 % strain of the material. Thus the hardness is a function of the yield stress (σ_y). It was found that [14] σ_y is given by;

$$\sigma_Y = \frac{VHN}{3.2} \quad \text{GPa} \qquad (1)$$

Table 4. Microhardness (Hv) and yield stress (σ_y) of melt quenched ribbons.

Alloy	Average of hardness readings $(Hv)_{98.07mN}$ (Gpa)	Yield stress (σ_y) (Gpa)
Sn_{70}-Bi_{15}-Sb_{15}	32.16	10.05
Sn_{68}-Bi_{15}-Sb_{15}- In_2	39.64	12.3875
Sn_{66}-Bi_{15}-Sb_{15}- In_4	52.28	16.3375
Sn_{64}-Bi_{15}-Sb_{15}- In_6	36.42	11.38125

Where VHN is in GPa. The details for Vickers micro hardness yield stress summarized in table for all prepared alloys are summarized in table (4).

From the table, it can be investigated that the maximum value of microhardness was for Sn_{66}-Bi_{15}-$Sb_{15}In_4$ prepared alloy and the least value for $Sn_{70}Bi_{15}Sb_{15}$ prepared alloy.

Elastic modulus (E), Shear modulus (G), Bulk modulus (B) and Poisson's ratio (υ) are calculated by dynamic resonance method for Sn_{70-x}-Sb_{15}-Bi_{15}-In_x alloys, x=0, 2, 4, and 6 at. %) [15,16]. It is investigated that (E) increases gradually with increasing the amount of In up to 33.6915 GPa to Sn_{64}-Sb_{15}-Bi_{15}-In_6 alloy. It has been found that the additions of In in SnSbBiIn as melt-quenched ribbons improve the elastic moduli and it is attributed to the substantial refinement of the solidification microstructure. The mechanical results are shown in Table (5).

Table 5. Young's modulus (E), Shear modulus (G), Bulk modulus (B) and Poisson's ratio (υ) for all prepared alloys.

Alloy	E (GPa)	B (GPa)	G (GPa)	υ
Sn_{70}-Bi_{15}-Sb_{15}	22.21295	25.35725	8.202716	0.354
Sn_{68}-Bi_{15}-Sb_{15}- In_2	26.10022	19.91319	10.18307	0.281
Sn_{66}-Bi_{15}-Sb_{15}- In_4	30.1586	22.28424	11.8321	0.274
Sn_{64}-Bi_{15}-Sb_{15}- In_6	33.69156	24.13401	13.29234	0.267

3. Conclusion

- It's found that, there are homogenous distributions of the alloying elements for all prepared alloys by melt spinning technique.
- Intermetallics such as Bi_3In_5 and InSb could be formed in the Sn-Bi-Sb melt-spun alloys. Structures of intermetallic SbSn and $In_{0.2}Sn_{0.8}$ form in Sn_{66}-Bi_{15}-Sb_{15}-In_4 alloy.
- Number of grain increase by increasing indium content.
- The change in micro-hardness depend the formation of intermetallic phase. From XRD result, it shown that $In_{0.2}Sn_{0.8}$ intermetallic compound exist only in Sn_{66}-Bi_{15}-Sb_{15}-In_4 alloy which showing the maximum value in microhardness.
- It is evident that in this work, the alloy which offers the best properties required for bearing applications is the rapidly solidified as-quenched melt-spun Sn_{66}-B_{i15}-S_{b15}-I_{n4} alloy. Since it has higher Young's modulus (30.15 GPa), higher hardness (52.28 Gpa) and higher yield stress (16.33 GPa).

Alloy (at.%)	E (GPa)	Hv (GPa)	σ_y (GPa)
Sn_{66}-B_{i15}-S_{b15}-I_{n4}	30.15	52.28	16.33

4. References

1. Wang, F., O'Keefe, M., Brinkmeyer, B., Journal of Alloys and Compounds 477(1–2): 267–273, 2009.
2. Wood, E.P., Nimmo, K.L., Journal of Electronic Materials 23(8):709-713, 1994.
3. Lead-Free Solder project, final report, National center for manufacturing science, Michigan, 1997.
4. Mustafa Kamal, Abu-Baker El-Bediwi and Tarek El-Ashram, Journal of Materials science in Electronics 15(2004) 211-217.
5. Rizk Mustafa Shalaby and Mustafa Kamal, International Journal of physic and Research (IJPR), Vol.13,Issues,Dec.(2013),51-60.
6. Mustafa Kamal, Shalabia Badr and Nermin Ali Abdelhakim, International Journal of Engineering and Technology IJET-IJENS Vol: 14, No: 01 Feb.(2014) IJENS, PP:119-129.
7. Mustafa Kamal, Abu-Baker El-Bediwi and Jamal Khalil Majeed, International Journal of Engineering and Technology IJET-IJENS Vol.14, No: 02 April(2014) IJENS, PP: 5 -15 .
8. Mustafa Kamal and Usama S. Mohammad, A Review: Chill- Block Melt Spin Technique, Theories & Applications, Bentham e Books, Bentham science Publishers eISBN:978-1-60805-151- 9,(2012).
9. A. Raouf, M. Kamal, T. El ashram, Sara Mosaad, Journal of Ovonic Research, Vol. 6, No. 6, November - December 2010, p. 297 – 302.

10. T. El ashram, M. Kamal, A. Raouf, S. Mosaad, Journal of Ovonic Research Vol. 8, No. 4, July - August 2012, p. 97 – 104.
11. B.D. Cullity," Elements of X-ray Diffraction", Addison–Wesley publishing company, INC, printed in the United States of American, (1959)PP: 263-265.
12. A.M. Shaban and M. Kamal, Radiation Effects and Defects in Solids, (1995),Vol.133, PP:5-13 .
13. Mustafa Kamal and Abu-Baker El-Bediwi, Radiation Effects and Defects in solids 174(1999)211.
14. M. Kamal, M. M. El-Tonsy, I. M. Fouda, M. Radwan, and H. M. Hosny, Bulletin of the Fac. Sci., Mansoura University Vol. 20(2) p. 1 (1993).
15. J.J.Gilman, Journal of Applied Physics,Vol.46,No.4,April (1975)PP: 1625-1633.
16. J.M. Ide,"Some Dynamic Methods of Determination of Young's Modulus", Rev. Sci. Instr.,6: 296 (1935).

Author' biography with photo

1. Sara Mosaad Mahlab
Ph.D. Student.
Assistant lecturer in Physics department,
Faculty of Science,
Suez Canal University,
Egypt.

2. Prof. Dr. Abd El- Raouf M.
Prof. of solid state physics, physics department,
Faculty of Science, Port-Said University,
Egypt.

3. Prof. Dr. Mustafa Kamal M. Youssef
Prof. of Metal Physics, Physics department,
Faculty of Science, Mansoura University,
Egypt.